Геология и геофизика, *2024, т. 65, № 12, с. 1752—1771*, DOI: 10.15372/GiG2024127, EDN: WXSAZI
Поступила в редакцию 01.03.2024, принята в печать 03.06.2024 *Опубликована онлайн: 06.06.2024*

УДК 553.551.4+551.762+552

ДЕТАЛЬНОЕ ИССЛЕДОВАНИЕ ДОЛОМИТОВ СРЕДНЕЮРСКОЙ СВИТЫ САМАНА СУК, РАЗРЕЗ КАХИ, БАССЕЙН НИЗАМПУР, СЕВЕРО-ЗАПАДНЫЕ ГИМАЛАИ (*Пакистан*)

А. Камал[1], М.М. Шах[1], Х. Рахим[1,2], Т. Зафар[3], Р. Халил[4], М.Ш. Шахзеб[1]

[1]*Department of Earth Sciences, Quaid-i-Azam University, Islamabad, 45320, Pakistan*

[2]*Earth Sciences Division, Pakistan Museum of Natural History, Islamabad, 44000, Pakistan*

[3]*Institute of Geochemistry, Chinese Academy of Sciences, Guiyang, 550081, China*

[4]*King Abdulaziz University, Jeddah, 21589, Saudi Arabia*

Диагенетически измененные карбонаты наиболее представительны среди горных пород. Многофазная доломитизация – наиболее распространенный из этих процессов. Среднеюрские карбонаты свиты Самана Сук (ССМС) интенсивно доломитизированы в разрезе Кахи в пределах бассейна Низампур. Главной целью настоящего исследования является изучение этой многофазной доломитизации и определение ее возможных механизмов. Полевые исследования включают как вмещающие известняки (оолитовые, содержащие ископаемые остатки и массивные), так и доломиты. Доломитовые тела залегают как параллельно слоистости, так и пересекают ее. Установлены различные типы доломитов на основе цветовых контрастов: темно-серые замещающие доломиты (RD), светло-серые доломиты, коричневатые и желтоватые доломиты. Помимо замещающей фазы, в полевых условиях также определены заполнение пустот и трещин, цементирующие седловидные доломиты (SD) и цементирующие кальцитовые тела (CC).

Петрографические исследования показывают сложную диагенетическую историю ССМС от приповерхностного диагенеза, включая микритизацию, неоморфизм, а также несколько следующих разновидностей доломитов. RD1 – от очень мелко- до мелкозернистого, RD2 – от средне- до грубозернистого, от гипидиоморфного до ксеноморфного, RD3 – от грубо- до очень грубозернистого планарный аутоморфный, зональный, RD4 – грубозернистый аутоморфный до гипидиоморфного железистого. Кроме того, цементирующие седловидные доломиты SD образуют крупные кристаллы, изогнутые грани с волнистым погасанием. Цементирующие кальцитовые фазы включают: CC1 – гранулярный мозаичный, CC2 – двойниковый, CC3 – заполняющий трещины, CC4 – железистый кальцит.

Значения стабильных изотопов известняка ($\delta^{18}O$: от –7.13 ‰ до –0.73 ‰ V-PDB и $\delta^{13}C$: от –0.05 ‰ до 1.32 ‰ V-PDB) указывают на деплетирование относительно юрской морской сигнатуры. Многофазные доломиты RD1–RD4 и значения для SD ($\delta^{18}O$: от –8.65 ‰ до –3.16 ‰ и $\delta^{13}C$: –3.56 ‰ до +2.09 ‰) указывают на многофазную доломитизацию. Значения для C1–C3 ($\delta^{18}O$: от –11.07 ‰ до –8.97 ‰ и $\delta^{13}C$: от –2.14 ‰ до +0.76 ‰) указывают на высоко деплетированные значения $\delta^{18}O$ и соответствуют гидротермальному источнику.

Полевые, петрографические и геохимические данные позволяют сделать вывод что возможным источником магния для гидротермальных доломитов была активация разломов и трещин во время активных тектонических движений в регионе, что может быть связано с активацией и реактивацией системы надвигов Кахи.

Доломиты, свита Самана Сук, средняя юра, петрография, стабильные изотопы

DETAILED INVESTIGATION OF DOLOMITES IN THE MIDDLE JURASSIC SAMANA SUK FORMATION, KAHI SECTION, NIZAMPUR BASIN, NW HIMALAYAS, PAKISTAN

A. Kamal, M.M. Shah, H.U. Rahim, T. Zafar, R. Khalil, M. Shahzeb

Diagenetically modified carbonate rocks are more common in the rock record. Among these modifications, multiphase dolomitization is the most common process. The Middle Jurassic carbonates of the Samana Suk Formation are extensively altered by the dolomitization process in the Kahi section, Nizampur Basin. The primary objective of this study is to investigate this multiphase dolomitization and to elucidate its possible mechanism.

Field investigation shows both host limestone (oolitic, fossiliferous, and massive) and dolomites. Dolomite bodies are of both beddings: parallel to and crosscutting the bedding planes. Different types of dolomites were recognized on the basis of color contrast as dark gray replacive dolomite, light gray dolomite, brownish dolomite, and yellowish dolomite. Along with the replacive phase, void- and fracture-filling cementing saddle dolomite and cementing calcites are recognized in the field. Petrographic studies show the complex diagenetic history of the Samana Suk Formation from near-surface diagenesis, including micritization, neomorphism, and several varieties of dolomites. These varieties are as follows: RD1 is very fine- to fine-grained dolomite; RD2 is medium- to coarse-grained and anhedral to subhedral dolomite; RD3 is coarse- to very coarse-grained and

✉e-mail: hamadrahim@gmail.com

planar euhedral zoned dolomite; and RD4 is coarse-grained euhedral to subhedral ferroan dolomite. In addition, cementing saddle dolomite SD consists of large crystals with curved faces showing sweeping extinction. Cementing calcite phases are as follows: CC1 is granular mosaic; CC2 is twin; CC3 is fracture-filling; and CC4 is ferroan calcite. The stable isotope values of limestone ($\delta^{18}O$ is –7.13 to –0.73‰ V-PDB, and $\delta^{13}C$ is –0.05 to 1.32‰ V-PDB) show depletion with respect to the Jurassic marine signature. The values of multiphase dolomites RD1–RD4 and SD ($\delta^{18}O$ is –8.65 to –3.16‰, and $\delta^{13}C$ is –3.56 to 2.09‰) indicate multiphase dolomitization. The CC1–CC3 values ($\delta^{18}O$ is –11.07 to –8.97‰, and $\delta^{13}C$ is –2.14 to 0.76‰) indicate highly depleted values of $\delta^{18}O$, showing hydrothermal origin. From field, petrography, and geochemistry data, it is deduced that a possible source of Mg for hydrothermal dolomites is activation of faults and fractures during active tectonic regime in the area and might be related to activation and reactivation of the Kahi Thrust system.

Dolomites, Middle Jurassic, petrography, stable isotopes, Samana Suk Formation

INTRODUCTION

Mineral dolomite is a double carbonate of calcium and magnesium having a rhombohedral crystal structure (Sibley and Gregg, 1987; Gregg et al., 2015). De Dolomieu in 1791 (de Dolomieu et al., 1981) was the first to discover and describe the rock as chiefly consisting of mineral dolomite. Mineral dolomite is the essential constituent of carbonate rocks bearing the identical name "dolomite." The chemical formula of dolomite is $CaMg(CO_3)_2$. Well-ordered stoichiometric dolomite consists of 50% mineral dolomite and 50% mineral calcite having alternate layers of Ca^{2+}–CO_3^{2-}–Mg^{2+}–CO_3^{2-}–Ca^{2+} (Machel and Mountjoy, 1986; Warren, 2000).

The mineral gains much attention, because dolomite hosts most of the hydrocarbon reservoirs and economic minerals, e.g., Mississippi Valley-type Pb and Zn deposits (Warren, 2000; Navarro-Ciurana et al., 2023). More than 50% of the whole world carbonate reservoirs are made up of dolomite (Zenger et al., 1980; Davies and Smith, 2006; Sharp et al., 2010). The processes of dolomitization are still an enigma amongst carbonate geologists (Morrow, 1982; Land, 1985; Machel and Mountjoy, 1986; Hardie, 1987; Budd, 1997; Arvidson and Mackenzie, 1999; Warren, 2000). During the past few decades, the origin of the mineral dolomite has remained a topic of intense debate amongst geoscientists. Most of present researchers agree on the secondary origin of dolomite and suggest that massive dolomites formed from the replacement of precursor limestone and rarely exist in nature as primary precipitated dolomite (Dickson, 1990; Morrow, 1990; Purser et al., 1994). In dolomitization processes, the precursor limestone is replaced by dolomite owing to the interaction of host rock with fluids of varying compositions in different diagenetic realms (Land, 1985; Machel and Mountjoy, 1986; Hardie, 1987; Vasconcelos and McKenzie, 1997; van Lith et al., 2002; Machel, 2004; Gasparrini et al., 2006; Dewit et al., 2012, 2014; Martín-Martín et al., 2013, 2015; Rahim et al., 2020, 2022). Fluids that are responsible for dolomitization are considered to be normal marine water (Saller, 1984; Carballo et al., 1987; Mazzullo, 2000), modified marine water (Baker and Kastner, 1981), marine water mixed with meteoric waters (Land, 1972; Magaritz et al., 1980; Cander, 1994), marine water mixed with salt brines (Meyers, 1991), and lacustrine water mixed with basinal brines (Machel, 2004). Most of these secondary dolomite bodies are either vertical or bedding-parallel and/or are mostly associated with some major faults (Nader and Swennen, 2004; Nader et al., 2007; Shah et al., 2010, 2012, 2016; Swennen et al., 2012; Dong et al., 2013; Navarro-Ciurana et al., 2016; Koeshidayatullah et al., 2020).

The Samana Suk Formation (SMSF) is present in the outcrops of the Nizampur Basin, Kala Chitta Range, Margala Hill Range, Hazara Basin, Salt Range, and Trans-Indus Range. The formation also contains dolomites in the Hazara Basin (Shah et al., 2016, 2020; Rahim et al., 2020, 2022; Shahzeb et al., 2024). However, there is no study of the dolomites of the Nizampur Basin. The proposed research aims to describe the types of dolomite and its formation mechanism through field, petrography, and isotopic study of a well-exposed succession of the Middle Jurassic SMSF in the Nizampur Basin, NW Pakistan. We identify the occurrence and distribution of dolomite and relative timing of different dolomite phases and propose a dolomitizing model for the Middle Jurassic SMSF.

GEOLOGIC SETTING

The Kahi section lies in the Nizampur Basin (Fig. 1). It is a part of the Himalayan fold-and-thrust belt situated in the foothill of the northwestern Himalayas of Pakistan (Fig. 1*a*). In the north, the Nizampur Basin is bounded by the Attock-Cherat Ranges and the Peshawar Basin (Fig. 1*b*; Burbank, 1982; Yaseen et al., 2021; Salam et al., 2024). The northeastern side of the Nizampur Basin is bounded by the Kherimar Hills and the Gandghar Ranges (Fig. 1*a*; Talent and Mawson, 1979). The Attock-Cherat Ranges surround the Nizampur Basin on the southern side and combine with the Kala Chitta Ranges (Yeats and Hussain, 1987). On the western

side, it is bounded by the Kala Chitta Hills. The Main Boundary Thrust (MBT) defines the southern boundary of the basin and thrusts the rocks of the Kala Chitta Ranges over the Kohat Plateau (Fig. 1*b*; McDougall et al., 1993; Salam et al., 2024).

The movement along these two major thrusts caused intense compressional deformation and shortening in the study area due to its presence near the MBT (Fig. 1*b*; Ghauri et al., 1991). The majority of the stratigraphic units in the study area are folded and thrusted. Owing to this intense deformation, the local-scale thrust faults and various large and small local-scale folds are also observed (Fig. 1*c*).

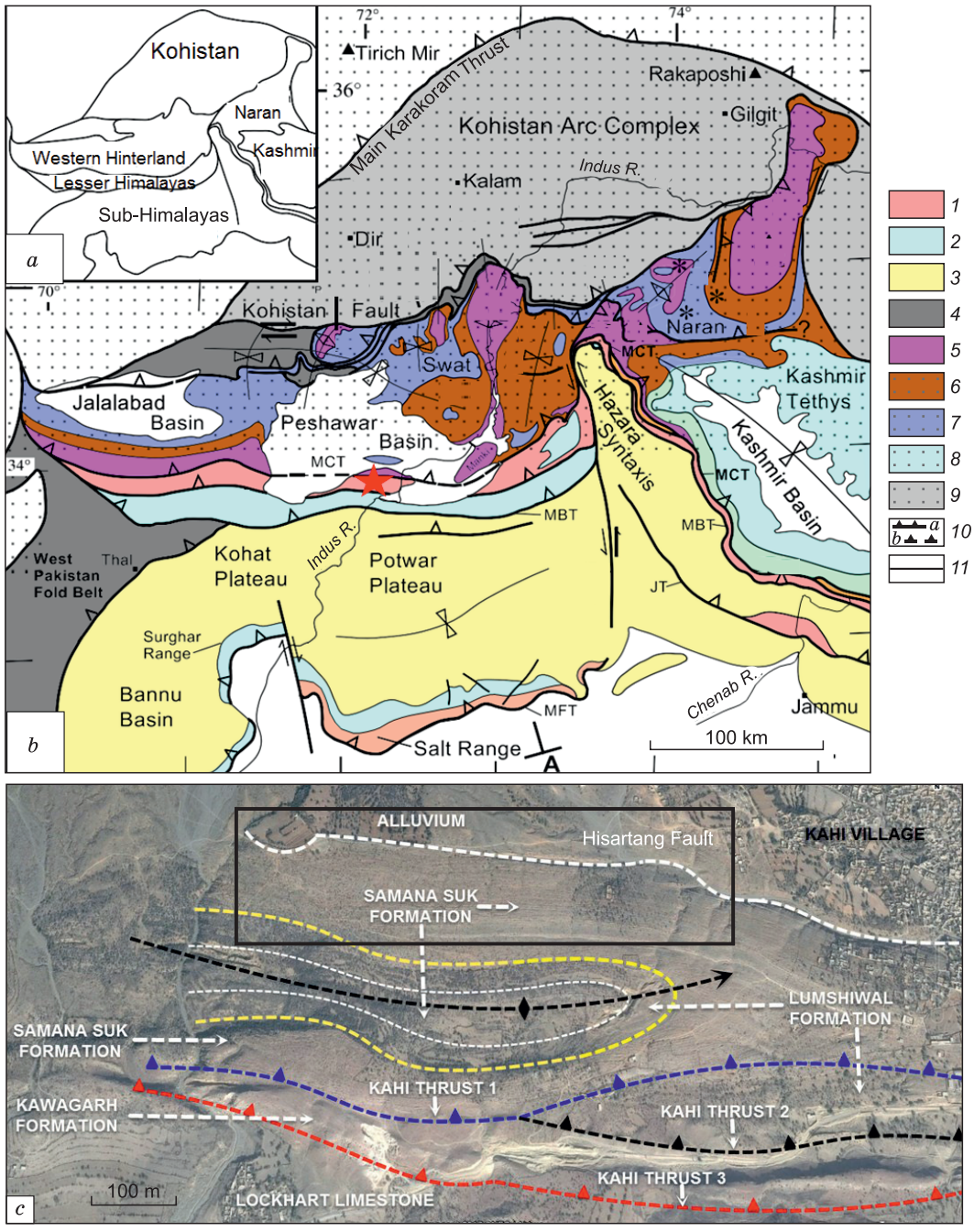

Fig. 1. *a* – Regional tectonic lines delineating different tectonic features; *b* – regional tectonic map of the NW Himalayas (modified after (DiPietro and Pogue, 2004)).

1 – Cambrian succession; *2* – Mesozoic succession; *3* – Potwar Plateau; *4* – Western Pakistan fold belt; *5* – Higher Himalayan metasediments; *6* – Higher Himalayan igneous rocks; *7* – Naran Swat area metasediments; *8* – Kashmir Tethys; *9* – Kohistan Arc Complex; *10* – *a* – confirmed fault; *b* – inferred fault; *11* – geologic contact. The study area is marked with a red star. MFT – Main Frontal Thrust; MBT – Main Boundary Thrust; JT – Jhelum Thrust; MCT – Main Central Thrust; *c* – Google Earth image showing different tectonic features of the study area. The measured section is marked with the box.

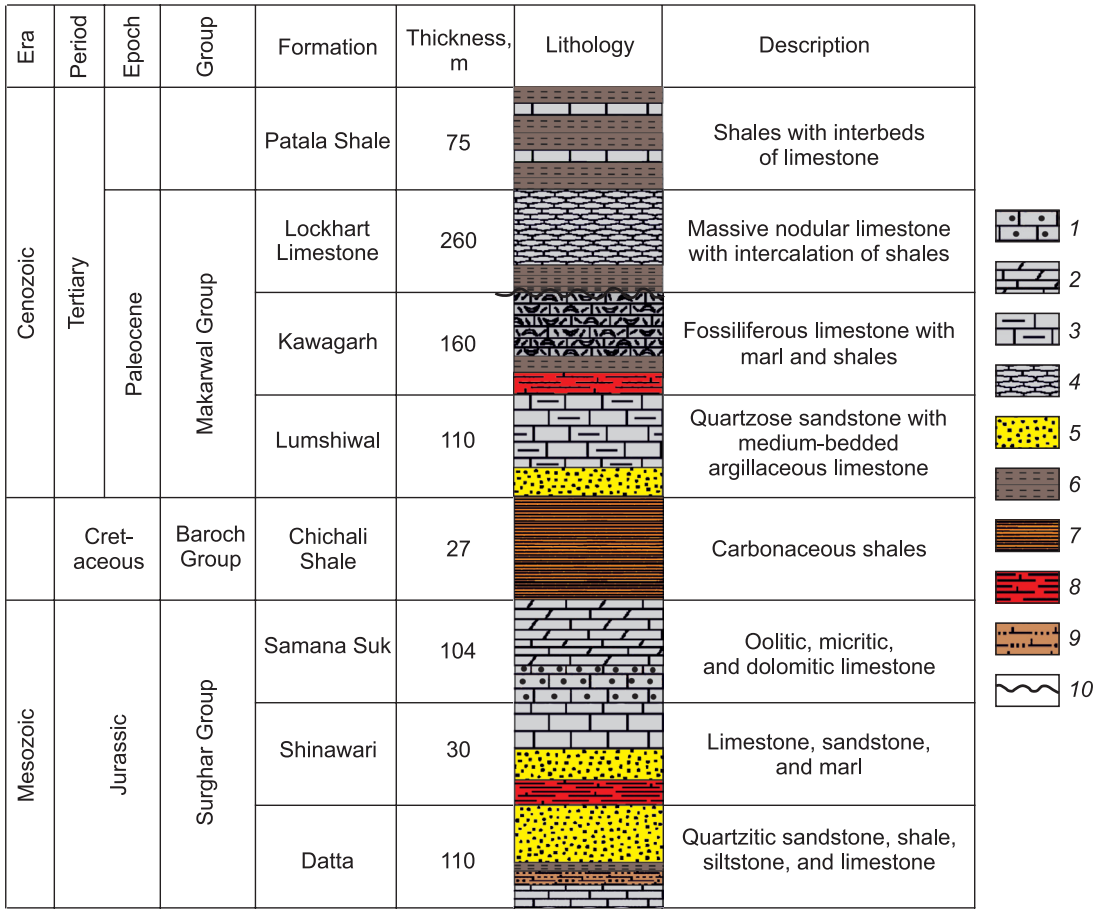

Fig. 2. The stratigraphic column of the Nizampur Basin, modified after (Shah, 2009).

1 – oolitic limestone; *2* – dolomitic limestone; *3* – argillaceous limestone; *4* – nodular limestone; *5* – sandstone; *6* – shale; *7* – carbonaceous shales; *8* – marl; *9* – siltstone; *10* – unconformity.

Stratigraphically, the Nizampur Basin represents rocks of Triassic, Jurassic, and Paleocene age (Fig. 2). By the mid-Mesozoic, the northwestern edge of the Indian Plate had been submerged within the Neo-Tethys Ocean, and this area was an important depocenter for carbonate deposition (Fig. 2; Kazmi and Jan, 1997). The Middle Jurassic epoch represents a time span for widespread carbonate deposition in shallow ramps and epeiric seas. This time span predominantly developed in the growth of shallow ooidal–peloidal banks in the Neo-Tethys Ocean (Al-Mojel et al., 2018). Such conditions in the Nizampur Basin in the Middle Jurassic (Bathonian–Callovian) time resulted in the deposition of the SMSF.

The formation is composed of gray to dark gray limestone with subordinate marl and shale intercalation. Limestone is mostly oolitic, which is the diagnostic feature of formation. In the studied outcrop, the formation is 104 m thick. The formation has a lower unconformable contact with the Jurassic sandstone of the Datta Formation and the upper unconformable contact with Cretaceous shales of the Chichali Formation (Fig. 2).

METHODS

The reconnaissance field work was carried out in the Nizampur Basin to study the dolomitization behavior and its intensity in the SMSF. The Kahi section in the Nizampur Basin was selected based on its accessibility, excellent outcrop exposure, and high intensity of dolomitization. In the detailed field studies, the formation was thoroughly examined and sampled from bottom to top. Fifty-six fresh samples of dolomites and limestone were collected from a 104-m-long section. Sampling was carried out based on textural and lithologic variations and the diagenetic features. Photography of sedimentary and diagenetic features was also carried out. Diluted HCl was used in the field to identify and differentiate limestone and dolomites. Finally, a samples description log was prepared, and the samples were brought to the laboratory.

The rock samples were cut in the lab, and slabs were prepared. For microscopic analysis, twenty-six representative samples were selected for thin sections. Thin sections were prepared in the lab of the Hydrocarbon Development Institute of Pakistan (HDIP). The Dickson (1966) method for staining was applied on the prepared thin sections. Alizarin Red-S and potassium ferricyanide were used for the staining purposes. With the help of staining, various calcite and dolomite phases were differentiated. Moreover, the crosscutting relationship and texture information were obtained. Thin sections were examined using a conventional polarizing microscope (Olympus CX31 with a DP-21 camera) at Quaid-i-Azam University (Islamabad).

For stable carbon and oxygen isotope analysis, different types of dolomite and calcite samples were taken with the help of a dental drill. Isotope analysis was carried out in the Isotope Application Division of Pakistan Institute of Nuclear Science and Technology (Islamabad). About 20 mg powder reacted with 100% phosphoric acid (density > 1.9 (Wachter and Hayes, 1985)) at 75 °C in an online carbonate preparation line (Carbo-Kiel—single-sample acid bath) connected to a Finnigan MAT 252 mass spectrometer. The dolomite isotopic composition values were corrected by the fractionation factors given by Rosenbaum and Sheppard (1986).

RESULTS

Outcrop observations revealed alternate beds of limestone and dolomites having variable thickness (Fig. 3*a*). Limestone beds are hard and compact, having off-white to grayish fresh color (Fig. 3*b*). Dolomite and limestone are differentiated on the basis of color appearance, brittle behavior, and effervescence intensity of the HCl test. Dolomitization in the SMSF varies from completely dolomitized and partially dolomitized to nondolomitized limestone (Fig. 3*c*).

At several places, within the same bed half the bed is dolomitized, and half the bed is remaining nondolomitized (Fig. 3*c*). At some places, precursor limestone is completely overprinted by dolomitization. No evidence of preservation of the original fabric and primary structures was found in the field (Fig. 3*d*, *e*). The contact between limestone and dolomite is represented by the dolomitizing front, which is usually irregular and wavy (Fig. 4*a*).

Both matrix and cementing dolomites are studied in the field. Cementing dolomite is mainly of saddle type showing typical baroque appearance and has positive relief from the surrounding rocks (Fig. 4*b*). Saddle dolomite is relatively coarse-grained, off-white in color. In the field studied saddle dolomite is characterized by yellowish weathered color and white fresh color (Fig. 4*e*, *f*).

Two types of calcite are identified in the field. These calcites are pore-filling cementing white calcite (Fig. 4*a*, *d*) and fracture-filling calcite (Fig. 4*b*). The white calcite is mainly associated with saddle dolomite (Fig. 4*d*), while fracture-filling calcite is crosscutting the stratification (Fig. 4*b*).

Stylolites are also abundant in the studied formation. Stylolites are found both in dolomite and limestone units (Fig. 3*d*, *e*). Both bedding-parallel and inclined stylolites are observed (Fig. 3*e*); however, the majority of stylolites are bedding-parallel (Fig. 3*d*, *e*). Pyrite mineral black in color is also found in association with stylolites and white calcite (Fig. 4*c*).

Petrography. The limestones of the SMSF are micritic, oolitic, and peloidal (Fig. 5*a*–*d*) with different types of dolomites (both fabric-preserving and fabric-obliterative) (Figs. 5, 6). Dolomites are classified on the basis of crystal size (very fine, fine, medium, and coarse), crystal texture (equigranular or inequigranular), crystal distribution (tightly or loosely packed, patches, isolated, and floating). Dolomite crystals are further classified into planar and nonplanar, euhedral and anhedral, and unimodal and polymodal (Figs. 5, 6; Randazzo and Zachos, 1984; Sibley and Gregg, 1987).

On the basis of microscopic study, four different replacive dolomites are recognized. Along with the replacive dolomite phase, one cementing saddle dolomite and two calcite phases are identified (Figs. 5, 6).

REPLACIVE DOLOMITE PHASES

Fine-grained matrix-selective dolomite RD1 is composed of anhedral to subhedral crystals 20–40 μm in size (rarely up to 60 μm) (Fig. 5*e*). Crystals of RD1 dolomite are usually free of inclusions. RD1 dolomite is fabric-obliterative and destroys the original rock fabric. Crystals are tightly packed and interlocked. RD1 dolomite lacks intercrystalline porosity owing to tight packing and interlocking of fine crystals. Secondary porosity present in the form of fractures, vugs, and molds is filled completely by cementing saddle dolomite SD (Fig. 5*e*).

The crystals of **medium- to coarse-grained matrix-selective subhedral dolomite RD2** are nonplanar subhedral. The crystal size ranges from 250 to 350 μm (Fig. 5*f*). RD2 dolomites are mostly fabric-obliterative. Crystals of RD2 dolomites are interlocked with curved intercrystal surfaces. In cross polarizing light, RD2 displays sharp extinction. RD2 crystals contain small inclusions and display cloudy appearance (Fig. 6*a*).

Coarse-grained planar euhedral zoned dolomite RD3 mostly consists of clear planar euhedral to subhedral crystals (Fig. 6*b*–*d*). The size of RD3 crystals ranges between 500 and 1000 μm. RD3 shows mosaic

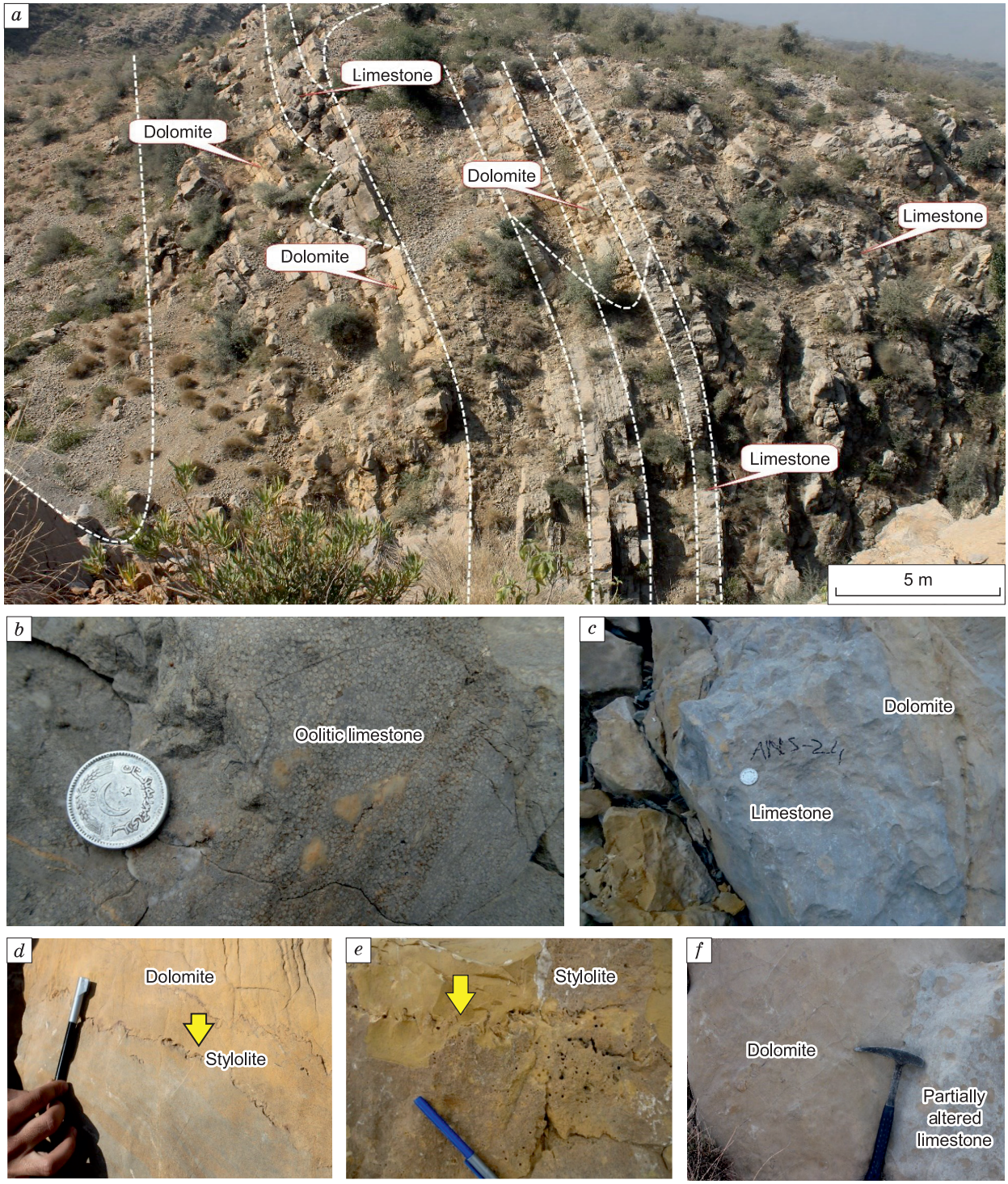

Fig. 3. Field photographs of the Kahi section showing exposures of the Samana Suk Formation (SMSF).

a – Panoramic photograph of the SMSF showing the orientation of beds with limestone and dolomite beds; *b* – oolitic limestone, which is typical of the formation; *c* – dolomite, limestone, and partially dolomitized limestone beds; *d* – brown dolomite crosscut by stylolite; dolomite types are separated by these stylolites; yellow arrow indicates the bedding-parallel stylolite; *e* – different types of dolomites; yellow arrow indicates the bedding-parallel stylolite; *f* – contact between dolomite and partially altered limestone. The alterations are mainly due to dolomitization.

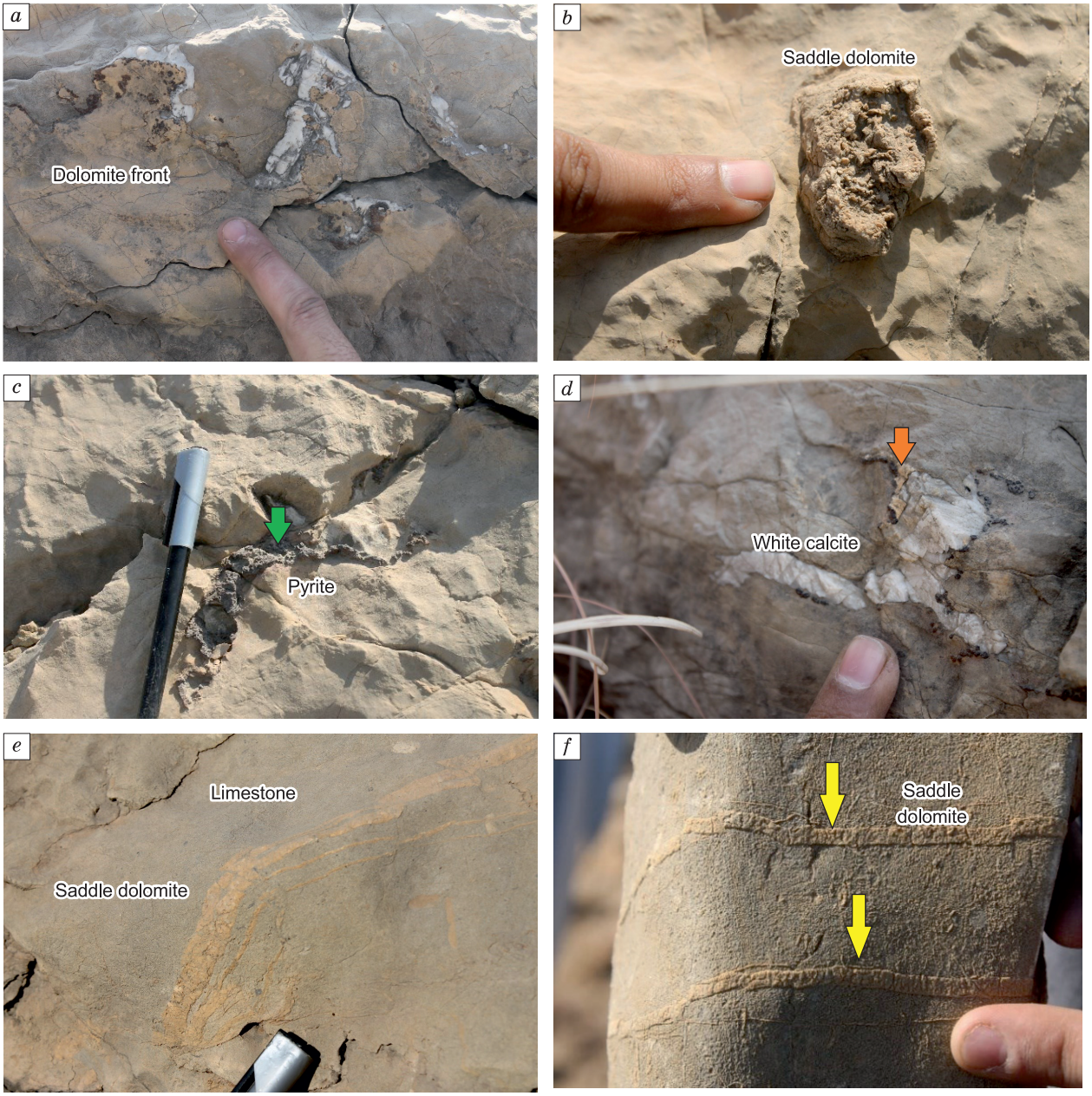

Fig. 4. Detailed field photographs of the Kahi section showing dolomites and other main diagenetic features:

a – dolomitizing front of wavy and irregular nature; *b* – saddle dolomite showing large crystal size and baroque appearance; *c* – pyrite mineralization showing rusty black appearance represented by the green arrow; *d* – white pore-filling calcite in contact with the saddle dolomite represented by the orange arrow; *e* – veins of saddle dolomite following the weak planes in the lithology; *f* – parallel veins of coarse-grained saddle dolomite are indicated by the yellow arrow.

textures of coarse-grained euhedral dolomite. Most of RD3 dolomites are zoned with a clear distinction from rim to core (Fig. 6*c*). The crystal cores and rims both have inclusions and display sharp extinction under cross polarized light. This type of dolomite is characterized by unimodal crystals. RD3 dolomites have intercrystalline porosity. The pores between the crystals are healed by brown iron oxides/pyrite (Fig. 6*c*).

Euhedral to subhedral ferroan dolomite RD4 is represented by coarse-grained euhedral to subhedral crystals (Fig. 6*e*, *f*). The crystals show mosaic texture. The crystals are inclusion-rich. Staining with K-ferricyanide and Alizarin Red-S helps to identify the ferroan variety of dolomite (Fig. 6*f*). RD4 crystals show strong extinction in cross polarized light. RD4 dolomite is a fabric-preserving variety, and original limestone fabric is

preserved. There is intercrystalline porosity in RD4; however, the intercrystalline porosity is filled with matrix material (Fig. 6*f*).

Saddle dolomite SD occurs as coarse- to very coarse-grained cementing dolomite and usually fills the pore spaces (Fig. 7*a*). The crystals are very large and range from 1000 to 5000 μm (Fig. 7*a*, *b*). The crystals are non-planar, having typical curved boundaries (Fig. 7*a*, *b*). Under cross polarizing light, SD displays undulous sweeping extinction (Fig. 7*a*, *b*).

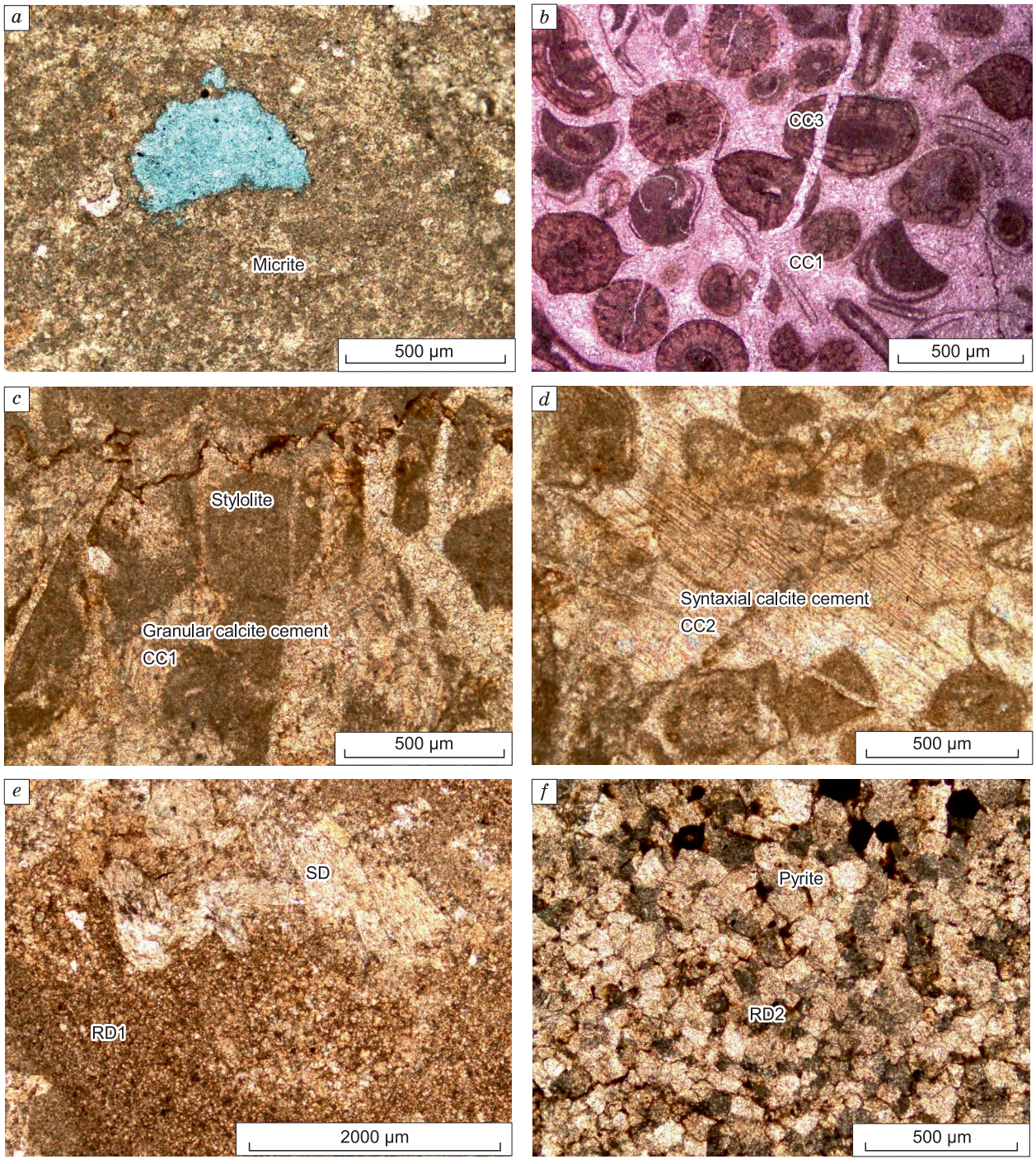

Fig. 5. XPL photomicrographs showing the diagenetic phenomenon in the SMSF:

a – micritic limestone with solution-enhanced pore spaces shown by the blue dye; *b* – oolitic limestone packed with fine-grained cement. CC1 is the marine phreatic cement, and CC3 is fracture-filling calcite cement. *c* – Limestone with peloidal texture. The fine-granular mosaic calcite cement (CC1) and bedding-parallel stylolite are also present; *d* – syntaxial calcite cement CC2 replacing the peloidal grains; *e* – very fine-grained dolomite RD1 in contact with saddle dolomite; *f* – medium- to coarse-grained fabric-obliterative dolomite RD2. Black pyrite crystals are also visible.

CALCITE CEMENTS

Fine crystalline calcite CC1 occurs as small anhedral crystals. CC1 has small to medium crystal size. CC1 forms equigranular mosaics within the allochems (Figs. 5*b*, 7*c*). Stained with Alizarin Red-S and potassium ferricyanide, CC1 appears pink (Fig. 7*c*). CC1 mostly forms druses of euhedral crystals. CC1 completely fills vuggy porosity.

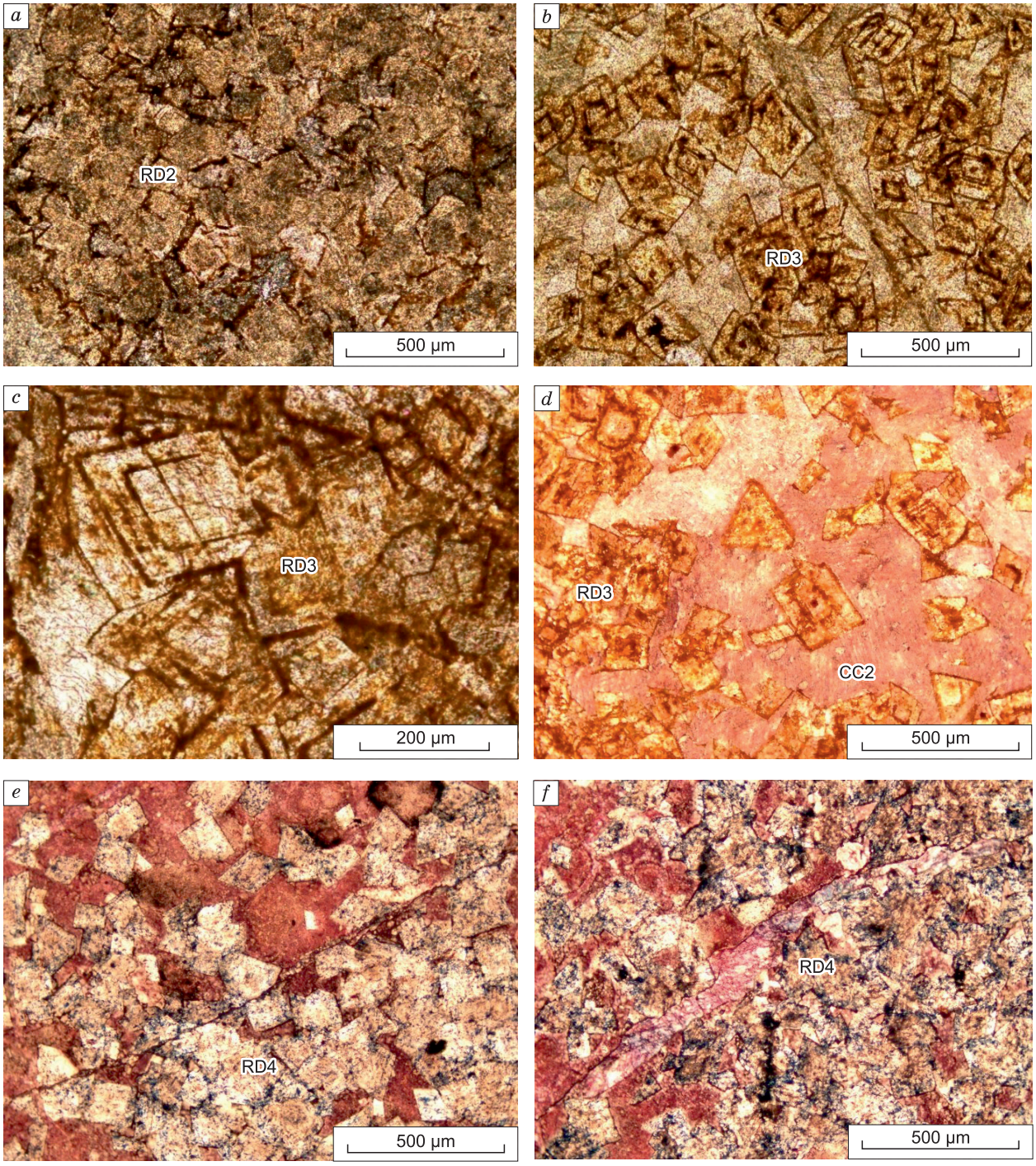

Fig. 6. Photomicrographs showing different dolomite phases.

a – Coarse-grained subhedral replacive dolomite RD2; *b* – coarse-grained planar euhedral zoned dolomite RD3. The crystals are perfectly formed and floating in the matrix. The zoned crystals have distinctive cores and rims. *c* – Detailed view of perfectly formed euhedral crystals of RD3; *d* – stained thin sections showing RD3 not influenced by Alizarin Red-S; *e* – euhedral crystals of ferroan dolomite; *f* – subhedral crystals of ferroan dolomite crosscut by fracture-filling calcite.

Twin white calcite CC2 has very large crystal size. The crystals are usually twinned with clear cleavage planes. The size of individual crystals exceeds 2000 μm (Fig. 7*d*, *f*). Twin calcite occurs in vugs, fractures, and veins of both dolomite and limestone.

Fracture-filling calcite CC3 is pink if stained with Alizarin Red-S. The crystals are small as compared to CC2. However, the size of an individual crystal ranges from 500 to 1000 μm. CC3 predates CC4, as observed in the crosscutting relationship (Fig. 7*c*).

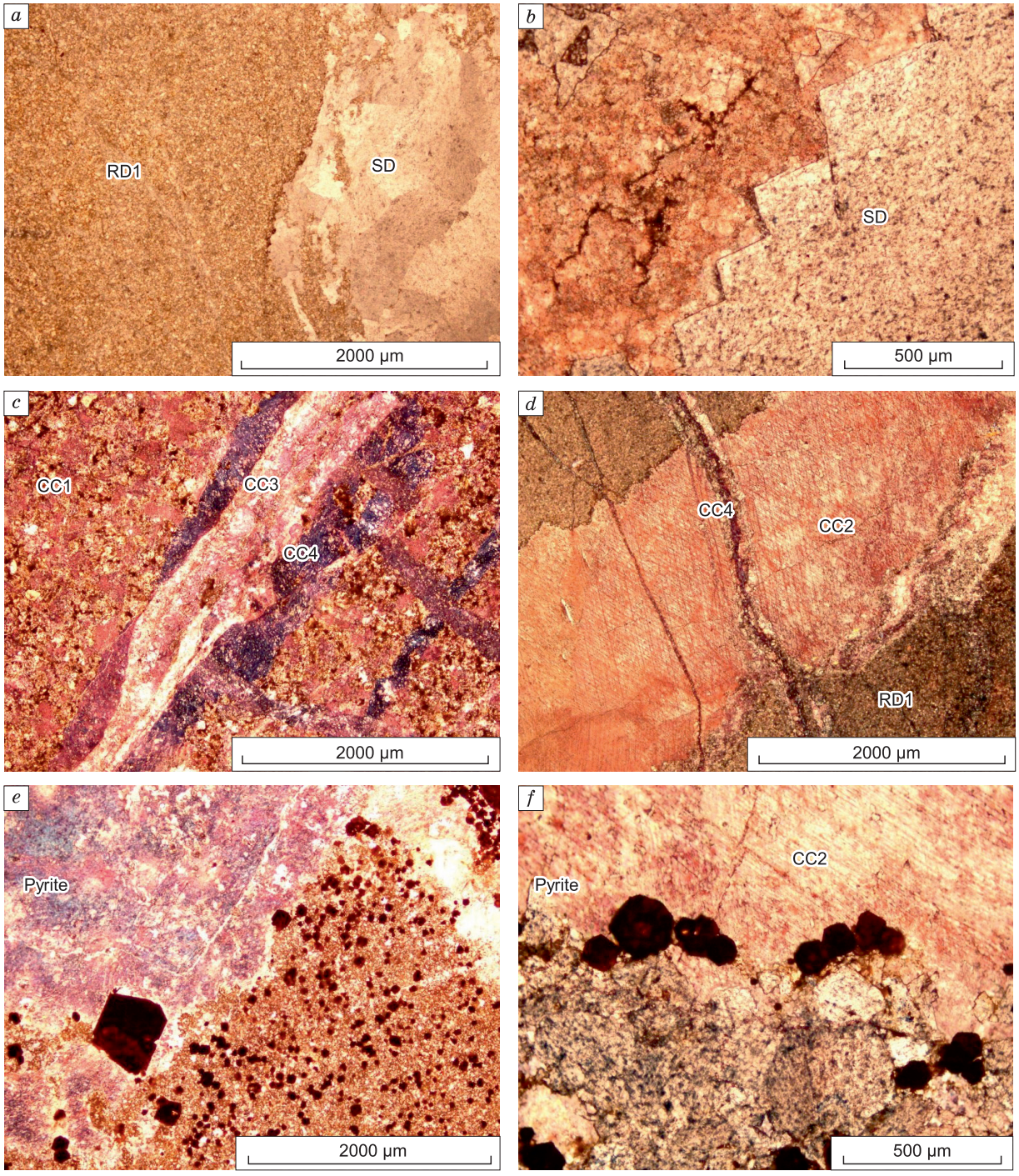

Fig. 7. Photomicrographs showing different diagenetic phases.

a – Saddle dolomite SD with large nonplanar crystals ranging in size from 1000 to 5000 μm; crystals are showing sweeping extinction in cross polarized light. SD is in contact with RD1. *b* – SD with curved crystal faces in a stained thin section. SD is in contact with host limestone affected by the staining. *c* – Different generations of calcite cements differentiated on the basis of staining. CC3 predating the CC4. CC4 is ferroan in nature, identified on the basis of blue staining color. *c* – View of a crosscutting relationship between CC2 and CC4; *e* – pyrites. Pyrite crystals are euhedral. *f* – Detailed view of brown pyrite of cubic crystal habit. The pyrites are in contact with SD and CC2.

Table 1. **Stable C and O isotope values of calcite and dolomite phases**

No.	Sample code	Phase	$\delta^{13}C$, ‰	$\delta^{18}O$, ‰
			(V-PDB)	(V-PDB)
1	ANS-3	RD1	–0.19	–4.79
2	ANS-6	RD3	2.07	–7.56
3	ANS-8	RD3	1.07	–6.97
4	ANS-13	RD2	–2.21	–7.15
5	ANS-18	RD2	–3.56	–7.26
6	ANS-20	Lst	0.06	–5.20
7	ANS-24	RD4	1.76	–8.65
8	ANS-28	RD4	2.09	–8.32
9	ANS-29	CC2	–0.08	–10.98
10	ANS-34	CC2	–1.87	–11.07
11	ANS-39	CC2	–2.14	–10.05
12	ANS-43	Lst	–0.05	–7.13
13	KS-4A	Lst	1.32	–0.73
14	KS-4B	RD1	0.21	–3.16
15	KS-4C	CC3	0.74	–8.51
16	KS-5	SD	0.50	–8.83
17	KS-6	SD	0.05	–10.00
18	KS-8	SD	0.30	–10.73
19	KS-11	CC3	0.56	–8.97
20	KS-12	CC3	0.76	–9.76

Note. The standard deviation of each measurement of $\delta^{13}C$ and $\delta^{18}O$ is ±0.1‰.

Ferroan calcite CC4 mainly occurs as cementing calcite. Stained ferroan calcite shows purple color (Fig. 7*c*, *e*). Ferroan calcite has large crystal size and usually occurs both in vugs and fractures, reducing secondary porosity. Ferroan calcite occurs in association with saddle dolomite and pyrites (Fig. 7*e*).

Other significant diagenetic features (stylolites and pyrites) were also recognized. Stylolites are found in abundance in the formation. The presence of stylolite is an indication of chemical compaction. Two different generations of stylolites are observed in petrographic study, i.e., older low-amplitude stylolites and younger high-amplitude stylolites crosscutting each other (Figs. 5*c*, 6*e*, 7*b*).

Pyrite mineralization is very common in the formation. Pyrites are mostly found as the replacive phase and mostly replace the dolomite crystals. The pyrite crystals are large, ranging in size from 200 to 500 μm (Fig. 7*e, f*). The crystals are brown to black and are mostly found in association with saddle dolomite and white calcite. In addition, large pyrite framboids are observed (Fig. 7*f*).

Stable C and O isotopes. The $\delta^{13}C$ and $\delta^{18}O$ values of various dolomite and calcite phases are listed in Table 1. Samples of different diagenetic phases show a wide variation of $\delta^{13}C$ and $\delta^{18}O$ values from Jurassic seawater indicative of diagenetic alteration in different environments (Fig. 8, Table 1). The isotopic values are compared with the known Jurassic signatures of Al-Mojel et al. (2018). The limestone $\delta^{13}C$ values range from –0.05 to 1.32‰ V-PDB, and the $\delta^{18}O$ values range from –7.13 to –0.73‰ V-PDB, showing depletion with respect to the Jurassic marine signature. The RD1 $\delta^{13}C$ value is –0.19‰ V-PDB, and $\delta^{18}O$ is –7.56‰ V-PDB. The RD2 $\delta^{13}C$ values ranging from –3.56‰ V-PDB to –2.21‰ V-PDB and the $\delta^{18}O$ values ranging from –7.26 to –7.15‰ V-PDB show depleted signatures of both carbon and oxygen. RD3 dolomite has $\delta^{13}C$ values ranging from 1.07‰ V-PDB to 2.07‰ V-PDB and $\delta^{18}O$ values of –7.56‰ V-PDB to –6.97‰ V-PDB, showing depletion in oxygen isotope values.

RD4 dolomite has $\delta^{13}C$ values which range from 1.76 to 2.09‰ V-PDB and $\delta^{18}O$ values which range from –8.65 to –8.32‰ V-PDB, showing depletion in oxygen isotope values. Saddle dolomite SD has $\delta^{13}C$ values of 0.05 to 0.50‰ V-PDB and $\delta^{18}O$ values which range from –10.73 to –8.83‰ V-PDB, showing depletion in oxygen isotopic values indicative of high temperature.

Cementing calcite CC2 has $\delta^{13}C$ isotopic values ranging from –2.14 to –0.08‰ V-PDB and $\delta^{18}O$ values of –11.07 to –10.05‰ V-PDB, showing the highest depleted values of $\delta^{18}O$. Fracture-filling calcite CC3 has $\delta^{13}C$ values ranging from 0.56 to 0.76‰ V-PDB and $\delta^{18}O$ values of –9.76 to –8.97‰ V-PDB, showing depleted values of $\delta^{18}O$ indicative of its formation from hot fluids. The $\delta^{18}O$ and $\delta^{13}C$ cross plot of various dolomite and calcite phases is shown in Fig. 9.

DISCUSSION

Paragenetic sequence. The SMSF carbonates of the Nizampur Basin have complex diagenetic history from its deposition to burial and uplift (Fig. 10). On the basis of field observations and petrographic studies, a detailed paragenetic sequence of the SMSF was established. The diagenetic stages like early, intermediate, and late are relative in nature, deduced on the basis of the crosscutting relationship among different phases, as reported in (Qing and Mountjoy, 1989, 1994; Chen et al., 2004; Machel, 2004; Dong et al., 2013; Rahim et al., 2020, 2024).

The near-surface diagenesis usually occurs in marine and meteoric conditions, which includes micritization, neomorphism, and dissolution of carbonate grains of the SMSF, as reported in (Rahim et al., 2020, 2022,

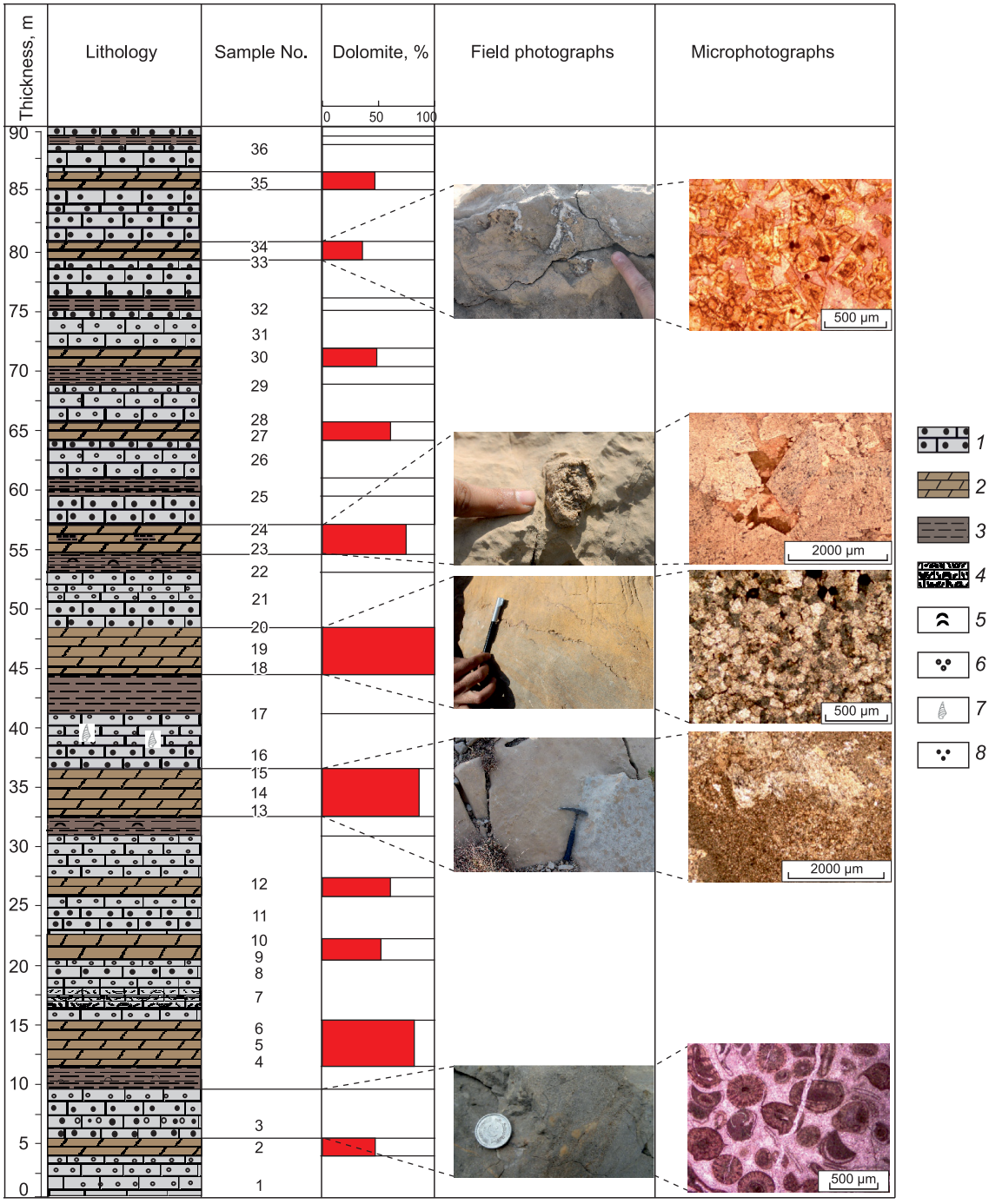

Fig. 8. Lithologic log of the SMSF showing dominant lithology as well as types of dolomites and their relative percentages within the sedimentary layers. The relative percentage of dolomite is developed based on the field and petrographic studies. The field and petrographic images showing different types of dolomites.

1 – oolitic limestone; *2* – dolomite; *3* – shale; *4* – fossiliferous limestone; *5* – bioclasts; *6* – ooids; *7* – gastropods; *8* – peloids.

2024; Rizwan et al., 2023; Shahzeb et al., 2024). This early marine diagenesis is also reported in the current study (Figs. 6*a–d*, 10). The diagenetic events predate mechanical and chemical compaction (Figs. 5*c*, 7*b*). Micritization is considered the earliest phase of diagenesis, which starts soon after the deposition of sediments (Swei and Tucker, 2012; Rizwan et al., 2023). The process is usually governed by the endolithic algae and bacteria (Rizwan et al., 2023).

The near-surface diagenesis is followed by episodes of shallow marine cementation. The shallow marine and meteoric conditions usually result in the formation of calcite cements within the framework grains (Rizwan et al., 2023; Shahzeb et al., 2024). The initial calcite cement in the SMSF is granular mosaic cement CC1, which represents typical meteoric-water conditions (Fig. 5*b*, *c*; Swei and Tucker, 2012). During these meteoric conditions, the formation of RD1 also occurs. The small size and subhedral shape of RD1 crystals demonstrate the conditions which are not of very high temperature (Montañez and Read, 1992). Instead, they represent the high supply of Mg. The main source of this huge Mg amount might have been modified seawater, as reported in (Montañez and Read, 1992; Kırmacı et al., 2018; Rahim et al., 2020).

The initial cementation event is followed by the shallow burial conditions, which resulted in the formation of syntaxial calcite cement and mechanical compaction of the grains (Fig. 5*c, d*).

Early shallow marine diagenesis of the SMSF is followed by replacive and cementing phases of dolomites and calcites. The first phase of replacement dolomites RD1 occurs as very fine- to fine-grained anhedral dolomite (Fig. 5*e*). RD1 replacement dolomite is followed by medium- to coarse-grained anhedral to subhedral dolomite RD2. The cooccurrence of medium- to coarse-grained replacement dolomite RD2 with fine-crystalline dolomite RD1 indicates that replacive dolomite RD2 formed from recrystallization of earlier formed replacive dolomite RD1 (Figs. 5*f*, 6*a*; Nader et al., 2007; Dong et al., 2013; Koeshidayatullah et al., 2020).

Replacive dolomites RD1 and RD2 are followed by the burial conditions which resulted in the formation of multiepisodic stylolites, as evidenced by the field and petrographic studies. Bedding-parallel stylolites usually indicate the burial-related chemical compaction of the lithology, and it is dominant in the carbonate rocks (Figs. 3*d, e*, 5*c*, 7*b;* Dong et al., 2013; Rahim et al., 2020). The fact that these stylolites are found in the dolomites clearly indicates that earlier dolomites formed prior to the stylolitization of the carbonate succession (Fig. 3*d*, *e*).

Coarse-crystalline syntaxial calcite CC2 fills the cavities formed in replacive dolomite RD1 (Fig. 7*d*, *f*). The syntaxial nature, due to the presence of cleavage planes, demonstrates that they were affected by the stresses related to the burial processes (Walker et al., 1990). RD3 and RD4 dolomites formed owing to burial-related processes. Their euhedral crystal shape demonstrates that they formed with the fluids highly saturated in Mg for a sufficient amount of time (Fig. 6*c–f*; Lind, 1993; Mountjoy and Amthor, 1994; Qing and Mountjoy, 1994; Duggan et al., 2001). The ferroan nature of RD4 also shows that Fe was in abundance during its formation. Iron concentration is usually high in the reducing conditions, which suggests their formation during the burial-related processes (Kırmacı et al., 2018).

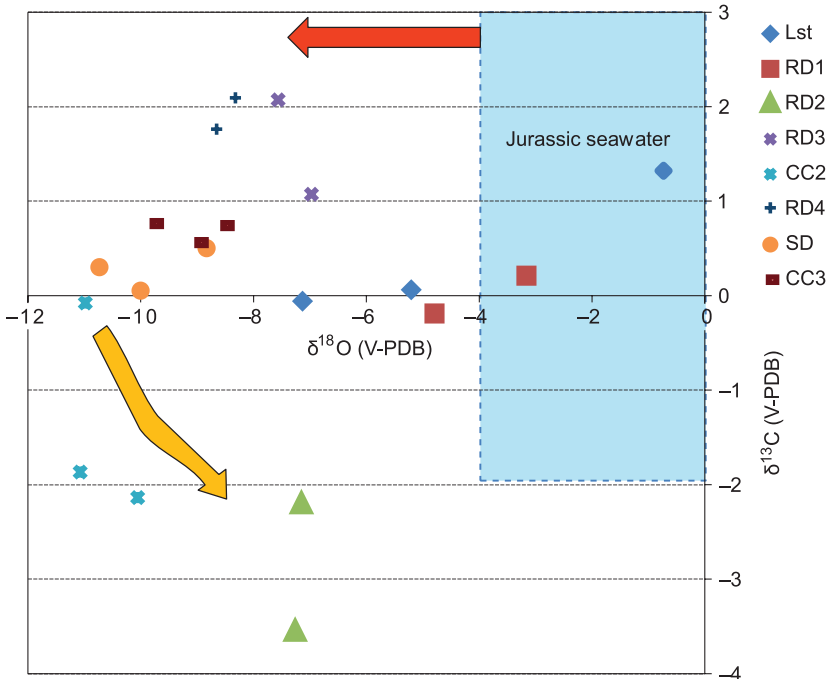

Fig. 9. Cross plot of stable C and O values of different diagenetic phases. Blue box indicates the isotopic values of Jurassic seawater (Al-Mojel et al., 2018). Red arrow pointed toward depleted $\delta^{18}O$ values is indicative of high temperature. Yellow arrow pointed toward depleted $\delta^{13}C$ values is indicative of possible meteoric influx.

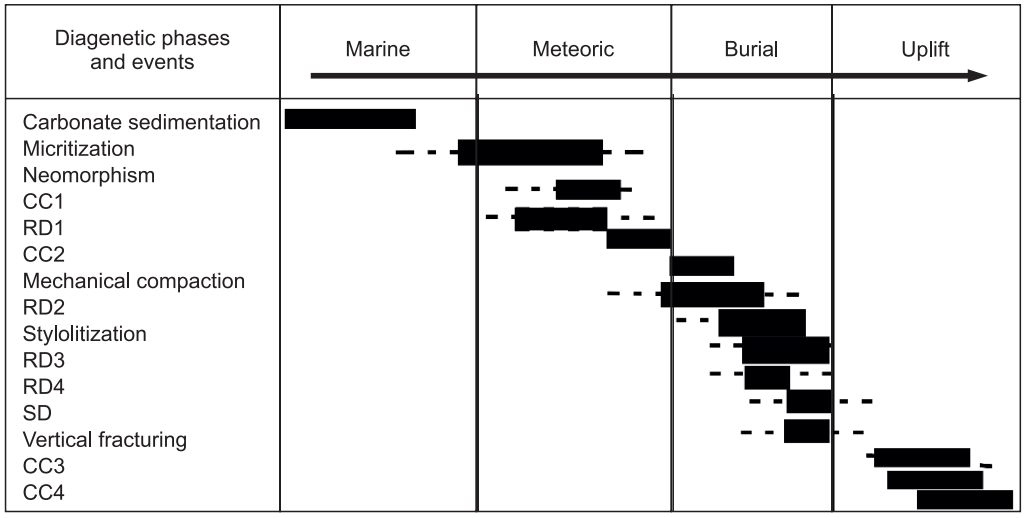

Fig. 10. Detailed paragenetic sequence of the SMSF carbonates in the Kahi section, Nizampur Basin.

The last burial diagenetic phase of the SMSF resulted in the formation of saddle dolomite SD owing to Mg-rich hydrothermal fluids percolating in the unfilled pore spaces of previous dolomitization phases (Fig. 4*b*). Saddle dolomite usually indicates the high temperature of its formation, as reported in (Gasparrini et al., 2006; Dong et al., 2013; Koeshidayatullah et al., 2020; Rahim et al., 2022).

In the uplift phases, fracture-filling calcite CC3 and ferroan calcite CC4 formed (Figs. 7*c*, *d*, 10). The steep-angle crosscutting relationship suggests that they formed during the last stages of the paragenetic sequence (Fig. 10). The steep-angle fracture-filling calcites are also found in the Paleogene succession and are related to the post-Eocene Himalayan orogeny (Rahim et al., 2024).

In the last uplift phase, replacive pyrite framboids formed. The typical cubic nature demonstrates the dysoxic conditions with abundant supply of sulfur (Liu et al., 2019). This is usually due to thermochemical sulfate reduction in the late burial diagenetic conditions. However, this sulfur might also be supplied owing to high-pressure conditions in tectonically active zones (Jiang et al., 2018). As the study area is tectonically active, it is deduced that the abundant sulfur was supplied owing to these overpressure conditions.

Mechanism of dolomitization. Detailed field observations and petrographic and geochemical studies of the SMSF show that dolomitization is a multiepisodic process and is demonstrated as follows.

Stage 1 includes the deposition of the host limestone, and early marine diagenetic events took place during this time (Fig. 11*a*). Micritization, neomorphism, and formation of RD1 and CC1 took place during this stage, because their stable isotopic signature lies within the range of the original Jurassic marine signatures (Fig. 9).

During **stage 2** the host limestone was subjected to shallow burial conditions by the ongoing deposition of a sedimentary package over the host limestone (Fig. 11*a*). This is supported by the presence of RD2 in association with RD1, because they are probably due to recrystallization of RD1. This stage is supported by the stable oxygen isotope values of the limestone, which are slightly negative, indicating the limestone burial conditions.

Activation of the fault took place during **stage 3** (Fig. 11*a*). This stage includes formation of replacive dolomites RD3 and RD4 in the host limestone; CC2 probably formed during this stage. The large crystal size and strongly depleted $\delta^{18}O$ values of RD3, RD4, and CC2 indicate that fluids with high temperature were involved in the formation of these dolomites and calcites. Also, these dolomites predate low-amplitude stylolite, which indicates their formation prior to reaching a depth of 500–600 m. The possible source of high-temperature fluid at such a shallow depth might be burial conditions, igneous activity, or a fault system (Gasparrini et al., 2006; Martín-Martín et al., 2015). Therefore, the formation time of replacement dolomites that formed before low-amplitude stylolites is not in accordance with the burial–compaction model. Field observation and tectonic history show no evidence of igneous activity in the study area. The absence of plutonic intrusions in the study area indicates that the source of high-temperature fluids was not igneous activity. The only possible source in the current scenario is the fault system present in the study area.

Stage 4. The faulting, nondepositional stage is followed by another stage of deposition of the Paleogene succession in the study area (Figs. 2, 11*a*). Owing to this burial, the deep-seated fluids rich in Mg penetrated the

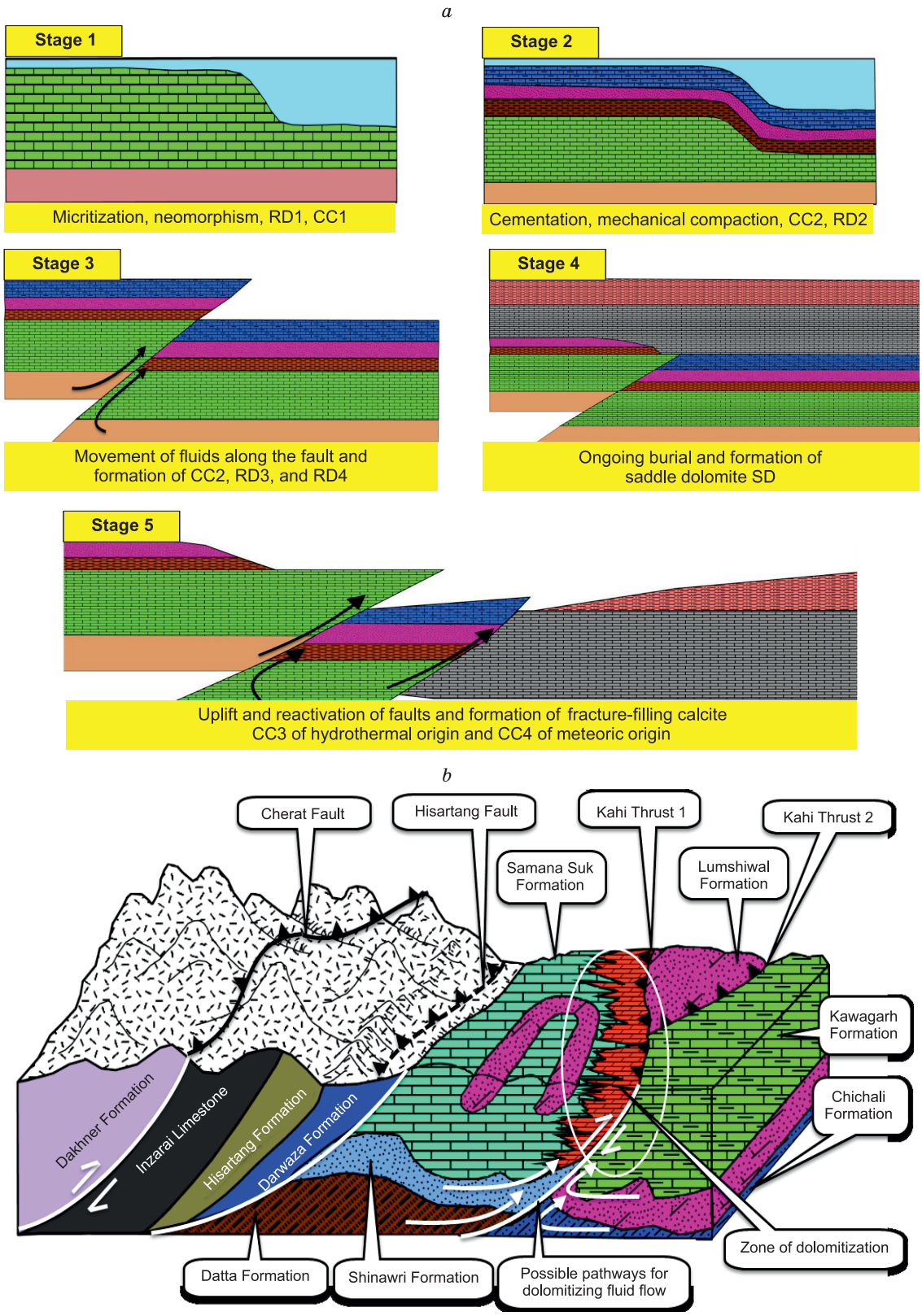

Fig. 11. ***a*** **– Model of evolutionary stages of the Nizampur Basin and the Kahi Mélange Complex, modified after (Salam et al., 2024). This tectonic setup resulted in the formation of multiphase dolomites in the SMSF.** ***b*** **– Block diagram showing the proposed dolomitizing model. Fault-related fluid flow is the main contributor to dolomitization in the study area.**

pore spaces, and this resulted in the formation of saddle dolomite SD. The well-developed large crystal faces and sweeping extinction demonstrate formation from the hydrothermal fluids. The depleted isotopic signatures also support this hypothesis, and the ferroan nature of RD4 indicates burial conditions after the previous uplifting and erosional stage.

Reactivation of the fault took place during **stage 5** owing to collision of the Indian and Eurasian plates (Fig. 11*a*). This stage includes calcite cement CC3 and CC4, along the fractures produced owing to this tectonic activity. CC3 has depleted isotopic signatures, and CC4 is ferroan calcite indicative of the involvement of high-temperature fluid in the precipitation of such cement. No evidence of stylolite crosscutting saddle dolomite SD and CC3 and ferroan calcite CC4 is observed, suggesting their formation during the late stage of uplift-related processes.

The study area was in a compressional zone; therefore, it underwent intense deformation. The pre-Paleocene deformation in the Attock-Cherat Ranges in the north of the study area caused intense deformation in the study area prior to the deposition of the Paleocene succession. As a result of push from the north, the Jurassic SMSF thrusted over Cretaceous successions. Possibly, the thrust system produced by pre-Paleocene deformation (Kahi Thrust 1 and Kahi Thrust 2) provided pathways for deep-seated fluids to move upward and cause dolomitization. Probably, the underlying siliciclastic sequence preserved fluids of marine nature, and, because of faulting, these fluids moved up and caused dolomitization of the Samana Suk Formation (Fig. 11). Probably, the activation and reactivation of the fault system contributed to providing fluids of different natures for multiphase dolomitization (Fig. 10*b*).

CONCLUSIONS

Field study of the SMSF indicates oolitic and micritic medium- to thick-bedded limestone, showing partially to completely dolomitized beds. In some parts, half the limestone bed is dolomitized, and half is nondolomitized limestone. The presence of partially dolomitized beds shows that dolomitization took place after the deposition of the limestone units.

Petrographic study of the SMSF indicates four matrix-replacive dolomites and one cementing saddle dolomite. These are fine-grained replacive dolomite (RD1), medium- to coarse-grained anhedral dolomite (RD2), coarse- to very coarse-grained euhedral dolomite (RD3), and coarse-grained euhedral to subhedral ferroan dolomite (RD4). Cementing dolomite is saddle dolomite (SD). Calcite cements include fine-grained cementing calcite CC1, twin calcite CC2, fracture-filling calcite CC3, and ferroan calcite CC4. The different sizes and crystal shapes of the dolomites and calcites indicate multiphase dolomitization and calcitization.

The stable isotope values of limestone ($\delta^{18}O$ is –7.13 to –0.73‰ V-PDB, and $\delta^{13}C$ is –0.05 to 1.32‰ V-PDB) show depletion with respect to the Jurassic marine signature. The values of multiphase dolomites RD1–RD4 and SD ($\delta^{18}O$ is –8.65 to –3.16‰, and $\delta^{13}C$ is –3.56 to 2.09‰) show multiphase dolomitization. The CC1–CC3 values ($\delta^{18}O$ is –11.07 to –8.97‰, and $\delta^{13}C$ is –2.14 to 0.76‰) indicate highly depleted values of $\delta^{18}O$, showing hydrothermal origin.

Petrographic and geochemical data on dolomite and calcite phases indicate multiphase dolomitization in the SMSF. The first phase, which includes replacive dolomites RD1, formed during the meteoric processes. RD2–RD4 formed owing to hydrothermal activity.

The fault and fracture system in the study area, including paleofaults, provided a pathway for the hydrothermal fluids to penetrate the succession and dolomitize the rocks. The possible source of fluids is from the aquifers in the sandstone units directly lying below the SMSF.

ACKNOWLEDGMENTS AND FUNDING

The Hydrocarbon Development Institute of Pakistan and Pakistan Institute of Nuclear Science and Technology (Islamabad) are acknowledged for preparation of thin sections and C/O isotope analysis.

We are thankful to the Higher Education Commission of Pakistan (HEC) for providing funds for the project. Partial support was provided by the HEC through the grant of Access to Scientific Instruments Program (ASIP 22/000813(HDIP, IBD/35)).

REFERENCES

Al-Mojel, A., Dera, G., Razin, P., Le Nindre, Y.M., 2018. Carbon and oxygen isotope stratigraphy of Jurassic platform carbonates from Saudi Arabia: Implications for diagenesis, correlations and global paleoenvironmental changes. Palaeogeogr. Palaeoclimatol. Palaeoecol. 511, 388–402, doi: 10.1016/j.palaeo.2018.09.005.

Arvidson, R.S., Mackenzie, F.T., 1999. The dolomite problem; control of precipitation kinetics by temperature and saturation state. Am. J. Sci. 299, 257–288, doi: 10.2475/ajs.299.4.257.

Baker, P.A., Kastner, M., 1981. Constraints on the formation of sedimentary dolomite. Science 213, 214–216, doi: 10.1126/science.213.4504.214.

Budd, D., 1997. Cenozoic dolomites of carbonate islands: their attributes and origin. Earth Sci. Rev. 42, 1–47, doi: 10.1016/S0012-8252(96)00051-7.

Burbank, D.W., 1982. The Chronology and Stratigraphic Evolution of the Kashmir and Peshawar Intermontane Basins, Northwestern Himalaya. Ph.D. Thesis. Dartmouth College.

Cander, H.S., 1994. An example of mixing-zone dolomite, middle Eocene Avon Park Formation, Floridan Aquifer system. J. Sediment. Res. 64, 615–629, doi: 10.1306/D4267E24-2B26-11D7-8648000102C1865D.

Carballo, J.D., Land, L.S., Miser, D.E., 1987. Holocene dolomitization of supratidal sediments by active tidal pumping, Sugarloaf Key, Florida. J. Sediment. Res. 57, 153–165, doi: 10.1306/212F8AD0-2B24-11D7-8648000102C1865D.

Chen, D., Qing, H., Yang, C., 2004. Multistage hydrothermal dolomites in the Middle Devonian (Givetian) carbonates from the Guilin area, South China. Sedimentology 51, 1029–1051, doi: 10.1111/j.1365-3091.2004.00659.x.

Davies, G.R., Smith, L.B., Jr., 2006. Structurally controlled hydrothermal dolomite reservoir facies: An overview. AAPG Bull. 90, 1641–1690, doi: 10.1306/05220605164.

De Dolomieu, D., Carozzi, A.V., Zenger, D.H., 1981. Sur un genre de pierres calcaires très-peu effervescentes avec les acides, & phosphorescentes par la collision. Translation with notes of Dolomieu's paper reporting his discovery of dolomite. J. Geol. Educ. 29, 4–10, doi: 10.5408/0022-1368-29.1.4.

Dewit, J., Huysmans, M., Muchez, P., Hunt, D.W., Thurmond, J.B., Vergés, J., Saura, E., Fernandez, N., Romaire, I., Esestime, P., Swennen, R., 2012. Reservoir characteristics of fault-controlled hydrothermal dolomite bodies: Ramales Platform case study, in: Garland, J., Neilson, J.E., Laubach, S.E., Whidden, K.J. (Eds.), Advances in Carbonate Exploration and Reservoir Analysis. Geol. Soc. London, Spec. Publ. 370, pp. 83–109, doi: 10.1144/SP370.1.

Dewit, J., Foubert, A., El Desouky, H.A., Muchez, P., Hunt, D., Vanhaecke, F., Swennen, R., 2014. Characteristics, genesis and parameters controlling the development of a large stratabound HTD body at Matienzo (Ramales Platform, Basque-Cantabrian Basin, northern Spain). Mar. Pet. Geol. 55, 6–25, doi: 10.1016/j.marpetgeo.2013.12.021.

Dickson, J.A.D., 1966. Carbonate identification and genesis as revealed by staining. J. Sediment. Res. 36, 491–505, doi: 10.1306/74D714F6-2B21-11D7-8648000102C1865D.

Dickson, T., 1990. Carbonate mineralogy and chemistry, in: Tucker, M.E., Wright, V.P. (Eds.), Carbonate Sedimentology. Blackwell, Oxford, pp. 284–313.

DiPietro, J.A., Pogue K.R., 2004. Tectonostratigraphic subdivisions of the Himalaya: A view from the west. Tectonics 23, doi: 10.1029/2003TC001554.

Dong, S., Chen, D., Qing, H., Zhou, X., Wang, D., Guo, Z., Qian, Y., 2013. Hydrothermal alteration of dolostones in the Lower Ordovician, Tarim Basin, NW China: multiple constraints from petrology, isotope geochemistry and fluid inclusion microthermometry. Mar. Pet. Geol. 46, 270–286, doi: 10.1016/j.marpetgeo.2013.06.013.

Duggan, J.P., Mountjoy, E.W., Stasiuk, L.D., 2001. Fault-controlled dolomitization at Swan Hills Simonette oil field (Devonian), deep basin west-central Alberta, Canada. Sedimentology 48, 301–323, doi: 10.1046/j.1365-3091.2001.00364.x.

Gasparrini, M., Bechstädt, T., Boni, M., 2006. Massive hydrothermal dolomites in the southwestern Cantabrian Zone (Spain) and their relation to the Late Variscan evolution. Mar. Pet. Geol. 23, 543–568, doi: 10.1016/j.marpetgeo.2006.05.003.

Ghauri, A.A.K., Pervez, M.K., Riaz, M., Rehman, O.U., Ahmad, I., Ahmad, S., 1991. The structure and tectonic setting of Attock-Cherat and Kalachitta Ranges in Nizampur area, N.W.F.P. Pakistan. Kashmir J. Geol. 8–9, 99–109.

Gregg, J.M., Bish, D.L., Kaczmarek, S.E., Machel, H.G., 2015. Mineralogy, nucleation and growth of dolomite in the laboratory and sedimentary environment: A review. Sedimentology 62, 1749–1769, doi: 10.1111/sed.12202.

Hardie, L.A., 1987. Dolomitization; a critical view of some current views. J. Sediment. Res. 57, 166–183, doi: 10.1306/212F8AD5-2B24-11D7-8648000102C1865D.

Jiang, L., Worden, R.H., Cai, C.F., Shen, A.J., He, X.Y., Pan, L.Y., 2018. Contrasting diagenetic evolution patterns of platform margin limestones and dolostones in the Lower Triassic Feixianguan Formation, Sichuan Basin, China. Mar. Pet. Geol. 92, 332–351, doi: 10.1016/j.marpetgeo.2017.10.029.

Kazmi, A.H., Jan, M.Q., 1997. Geology and Tectonics of Pakistan. Graphic Publishers, Karachi.

Kırmacı, M.Z., Yıldız, M., Kandemir, R., Eroğlu-Gümrük, T., 2018. Multistage dolomitization in Late Jurassic–Early Cretaceous platform carbonates (Berdiga Formation), Başoba Yayla (Trabzon), NE Turkey: Implications of the generation of magmatic arc on dolomitization. Mar. Pet. Geol. 89, 515–529, doi: 10.1016/j.marpetgeo.2017.10.018.

Koeshidayatullah, A., Corlett, H., Stacey, J., Swart, P.K., Boyce, A., Robertson, H., Whitaker, F., Hollis, C., 2020. Evaluating new fault-controlled hydrothermal dolomitization models: insights from the Cambrian Dolomite, Western Canadian Sedimentary Basin. Sedimentology 67, 2945–2973, doi: 10.1111/sed.12729.

Land, L.S., 1972. Contemporaneous dolomitization of Middle Pleistocene reefs by meteoric water, North Jamaica. AAPG Bull. 56, 635, doi: 10.1306/819A3F9A-16C5-11D7-8645000102C1865D.

Land, L.S., 1985. The origin of massive dolomite. J. Geol. Educ. 33, 112–125, doi: 10.5408/0022-1368-33.2.112.

Lind, I., 1993. Stylolites in chalk from Leg 130, Ontong Java Plateau, in: Berger, W.H., Kroenke, J.W., Mayer, L.A., et al. (Eds.), Proceedings of the Ocean Drilling Program, Scientific Results, pp. 445–451, doi: 10.2973/odp.proc.sr.130.006.1993.

Liu, Z., Chen, D., Zhang, J., Lü, X., Wang, Z., Liao, W., Shi, X., Tang, J., Xie, G., 2019. Pyrite morphology as an indicator of paleoredox conditions and shale gas content of the Longmaxi and Wufeng shales in the middle Yangtze area, south China. Minerals 9, 428, doi: 10.3390/min9070428.

Machel, H.G., 2004. Concepts and models of dolomitization: a critical reappraisal, in: Braithwaite, C.J.R., Rizzi, G., Darke, G. (Eds.), The Geometry and Petrogenesis of Dolomite Hydrocarbon Reservoir. Geol. Soc. London, Spec. Publ. 235, pp. 7–63, doi: 10.1144/GSL.SP.2004.235.01.02.

Machel, H.G., Mountjoy, E.W., 1986. Chemistry and environments of dolomitization—a reappraisal. Earth Sci. Rev. 23, 175–222, doi: 10.1016/0012-8252(86)90017-6.

Magaritz, M., Goldenberg, L., Kafri, U., Arad, A., 1980. Dolomite formation in the seawater–freshwater interface. Nature 287, 622–624, doi: 10.1038/287622a0.

Martín-Martín, J.D., Gomez-Rivas, E., Bover-Arnal, T., Travé, A., Salas, R., Moreno-Bedmar, J.A., Tomás, S., Corbella, M., Teixell, A., Vergés, J., Stafford, S.L., 2013. The Upper Aptian to Lower Albian syn-rift carbonate succession of the southern Maestrat Basin (Spain): Facies architecture and fault-controlled stratabound dolostones. Cretaceous Res. 41, 217–236, doi: 10.1016/j.cretres.2012.12.008.

Martín-Martín, J.D., Travé, A., Gomez-Rivas, E., Salas, R., Sizun, J.-P., Vergés, J., Corbella, M., Stafford, S.L., Alfonso, P., 2015. Fault-controlled and stratabound dolostones in the Late Aptian–earliest Albian Benassal Formation (Maestrat Basin, E Spain): Petrology and geochemistry constrains. Mar. Pet. Geol. 65, 83–102, doi: 10.1016/j.marpetgeo.2015.03.019.

Mazzullo, S., 2000. Organogenic dolomitization in peritidal to deep-sea sediments. J. Sediment. Res. 70, 10–23, doi: 10.1306/2DC408F9-0E47-11D7-8643000102C1865D.

McDougall, J.W., Hussain, A., Yeats, R.S., 1993. The Main Boundary Thrust and propagation of deformation into the foreland fold-and-thrust belt in northern Pakistan near the Indus River. Geol. Soc. London, Spec. Publ. 74, 581–588, doi: 10.1144/GSL.SP.1993.074.01.38.

Meyers, W.J., 1991. Calcite cement stratigraphy: An overview, in: Barker, C.E., Burruss, R.C., Kopp, O.C., Machel, H.G., Marshall, D.J., Wright, P., Colbum, H.Y. (Eds.), Luminescence Microscopy and Spectroscopy: Qualitative and Quantitative Applications. SEPM Short Course No. 25, doi: 10.2110/scn.91.25.0133.

Montañez, I.P., Read, J.F., 1992. Fluid-rock interaction history during stabilization of early dolomites, Upper Knox Group (Lower Ordovician), US Appalachians. J. Sediment. Res. 62, 753–778, doi: 10.1306/D42679D3-2B26-11D7-8648000102C1865D.

Morrow, D., 1982. Diagenesis 1. Dolomite - Part 1: The chemistry of dolomitization and dolomite precipitation. Geosci. Can. 9, 5–13.

Morrow, D., 1990. Part 1: The chemistry of dolomitization and dolomite precipitation, in: McIlreath, I.A., Morrow, D.W. (Eds.), Diagenesis. Geosci. Can., Ser. 4, 113–124.

Mountjoy, E.W., Amthor, J.E., 1994. Has burial dolomitization come of age? Some answers from the western Canada sedimentary basin, in: Purser, B., Tucker, M., Zenger, D. (Eds.), Dolomites. A Volume in Honour of Dolomieu. Int. Assoc. Sedimentol. Spec. Publ. 21, pp. 203–229, doi: 10.1002/9781444304077.ch13.

Nader, F.H., Swennen, R., 2004. The hydrocarbon potential of Lebanon: New insights from regional correlations and studies of Jurassic dolomitization. J. Pet. Geol. 27, 253–275, doi: 10.1111/j.1747-5457.2004.tb00058.x.

Nader, F.H., Swennen, R., Ellam, R., 2007. Field geometry, petrography and geochemistry of a dolomitization front (Late Jurassic, central Lebanon). Sedimentology 54, 1093–1119, doi: 10.1111/j.1365-3091.2007.00874.x.

Navarro-Ciurana, D., Corbella, M., Cardellach, E., Vindel, E., Gómez-Gras, D., Griera, A., 2016. Petrography and geochemistry of fault-controlled hydrothermal dolomites in the Riópar area (Prebetic Zone, SE Spain). Mar. Pet. Geol. 71, 310–328, doi: 10.1016/j.marpetgeo.2016.01.005.

Navarro-Ciurana, D., Corral, I., Corbella, M., 2023. A tool for Zn-Pb MVT exploration by combining C and O isotopes and REE geochemistry of dolomite. Ore Geol. Rev. 156, 105405, doi: 10.1016/j.oregeorev.2023.105405.

Purser, B.H., Tucker, M.E., Zenger, D.H. (Eds.), 1994. Dolomites - A Volume in Honour of Dolomieu. Int. Assoc. Sedimentol., Spec. Publ. 21.

Qing, H., Mountjoy, E.W., 1989. Multistage dolomitization in Rainbow buildups, Middle Devonian Keg River Formation, Alberta, Canada. J. Sediment. Res. 59, 114–126, doi: 10.1306/212F8F30-2B24-11D7-8648000102C1865D.

Qing, H., Mountjoy, E.W., 1994. Formation of coarsely crystalline, hydrothermal dolomite reservoirs in the Presqu'ile barrier, Western Canada Sedimentary Basin. AAPG Bull. 78, 55–77, doi: 10.1306/BDFF9014-1718-11D7-8645000102C1865D.

Rahim, H.U., Shah, M.M., Corbella, M., Navarro-Ciurana, D., 2020. Diagenetic evolution and associated dolomitization events in the middle Jurassic Samana Suk Formation, lesser Himalayan Hill Ranges, NW Pakistan. Carbonates Evaporites 35, 101, doi: 10.1007/s13146-020-00634-0.

Rahim, H.U., Qamar, S., Shah, M.M., Corbella, M., Martín-Martín, J.D., Janjuhah, H.T., Navarro-Ciurana, D., Lianou, V., Kontakiotis, G., 2022. Processes associated with multiphase dolomitization and other related diagenetic events in the Jurassic Samana Suk Formation, Himalayan Foreland Basin, NW Pakistan. Minerals 12, 1320, doi: 10.3390/min12101320.

Rahim, H.U., Ahmad, W., Jamil, M., Khalil, R., 2024. Sedimentary facies, diagenetic analysis, and sequence stratigraphic control on reservoir evaluation of Eocene Sakesar limestone, Upper Indus basin, NW Himalayas. Carbonates Evaporites 39, 15, doi: 10.1007/s13146-024-00947-4.

Randazzo, A.F., Zachos, L.G., 1984. Classification and description of dolomitic fabrics of rocks from the Floridan aquifer, U.S.A. Sediment. Geol. 37, 151–162, doi: 10.1016/0037-0738(84)90005-8.

Rizwan, M., Hanif, M., Ullah, S., Ishaq, M., 2023. Detailed diagenetic investigation and their impact on the reservoir potential of Upper Cretaceous mixed carbonate-siliciclastic succession, Rakhi Nala Section, Eastern Sulaiman Range, Pakistan. Carbonates Evaporites 38, 50, doi: 10.1007/s13146-023-00871-z.

Rosenbaum, J., Sheppard, S.M.F., 1986. An isotopic study of siderites, dolomites and ankerites at high temperatures. Geochim. Cosmochim. Acta 50, 1147–1150, doi: 10.1016/0016-7037(86)90396-0.

Salam, H., Turab, S.A., Ali, A., Jan, M.Q., Sulaiman, N., Basori, M.B.I., 2024. Kahi mélange complex in Kurram and Waziristan, NW Pakistan: An integrated approach for tectonic implications to India–Afghan suturing. Gondwana Res. 126, 79–95, doi: 10.1016/j.gr.2023.10.001.

Saller, A.H., 1984. Petrologic and geochemical constraints on the origin of subsurface dolomite, Enewetak Atoll: An example of dolomitization by normal seawater. Geology 12, 217–220, doi: 10.1130/0091-7613(1984)12<217:PAGCOT>2.0.CO;2.

Shah, M.M., Nader, F.H., Dewit, J., Swennen, R., Garcia, D., 2010. Fault-related hydrothermal dolomites in Cretaceous carbonates (Cantabria, northern Spain): Results of petrographic, geochemical and petrophysical studies. Bull. Soc. Géol. Fr. 181, 391–407, doi: 10.2113/gssgfbull.181.4.391.

Shah, M.M., Nader, F.H., Garcia, D., Swennen, R., Ellam, R., 2012. Hydrothermal dolomites in the Early Albian (Cretaceous) platform carbonates (NW Spain): Nature and origin of dolomites and dolomitising fluids. Oil Gas Sci. Technol., IFP Energies nouvelles, 67, 97–122, doi: 10.2516/ogst/2011174.

Shah, M.M., Ahmed, W., Ahsan, N., Lisa, M., 2016. Fault-controlled, bedding-parallel dolomite in the middle Jurassic Samana Suk Formation in Margalla Hill Ranges, Khanpur area (North Pakistan): petrography, geochemistry, and petrophysical characteristics. Arabian J. Geosci. 9, 405, doi: 10.1007/s12517-016-2413-y.

Shah, M.M., Rahim, H.U., Hassan, A., Mustafa, M.R., Ahmad, I., 2020. Facies control on selective dolomitization and its impact on reservoir heterogeneities in the Samana Suk Formation (middle Jurassic), Southern Hazara Basin (NW Himalaya, Pakistan): an outcrop analogue. Geosci. J. 24, 295–314, doi: 10.1007/s12303-019-0026-7.

Shah, S.M.I., 2009. Stratigraphy of Pakistan. Geol. Surv. Pak. Mem. 22, 1–381.

Shahzeb, M., Shah, M.M., Rahim, H.U., Jan, J.A., Ahmad, I., Khalil, R., Shehzad, K., 2024. Depositional and diagenetic studies of the middle Jurassic Samana Suk Formation in the Trans Indus Ranges and western extension of Hill Ranges, Pakistan: an integrated sedimentological and geochemical approach. Carbonates Evaporites 39, 19, doi: 10.1007/s13146-024-00937-6.

Sharp, I., Gillespie, P., Morsalnezhad, D., Taberner, C., Karpuz, R., Vergés, J., Horbury, A., Pickard, N., Garland, J., Hunt, D., 2010. Stratigraphic architecture and fracture-controlled dolomitization of the

Cretaceous Khami and Bangestan groups: an outcrop case study, Zagros Mountains, Iran. Geol. Soc. London, Spec. Publ. 329, 343–396, doi: 10.1144/SP329.14.

Sibley, D.F., Gregg, J.M., 1987. Classification of dolomite rock textures. J. Sediment. Res. 57, 967–975, doi: 10.1306/212F8CBA-2B24-11D7-8648000102C1865D.

Swei, G., Tucker, M.E., 2012. Impact of diagenesis on reservoir quality in ramp carbonates: Gialo Formation (Middle Eocene), Sirt Basin, Libya. J. Pet. Geol. 35, 25–47, doi: 10.1111/j.1747-5457.2012.00517.x.

Swennen, R., Dewit, J., Fierens, E., Muchez, P., Shah, M., Nader, F.H., Hunt, D., 2012. Multiple dolomitization events along the Pozalagua Fault (Pozalagua Quarry, Basque–Cantabrian Basin, Northern Spain). Sedimentology 59, 1345–1374, doi: 10.1111/j.1365-3091.2011.01309.x.

Talent, J.A., Mawson, R., 1979. Paleozoic-Mesozoic biostratigraphy of Pakistan in relation to biogeography and the coalescence of Asia, in: Farah, A., DeJong, K. (Eds.), Geodynamics of Pakistan. GSP, Quetta, 81–102.

van Lith, Y., Vasconcelos, C., Warthmann, R., Martins, J., McKenzie, J., 2002. Bacterial sulfate reduction and salinity: two controls on dolomite precipitation in Lagoa Vermelha and Brejo do Espinho (Brazil). Hydrobiologia 485, 35–49, doi: 10.1023/A:1021323425591.

Vasconcelos, C., McKenzie, J.A., 1997. Microbial mediation of modern dolomite precipitation and diagenesis under anoxic conditions (Lagoa Vermelha, Rio de Janeiro, Brazil). J. Sediment. Res. 67, 378–390, doi: 10.1306/D4268577-2B26-11D7-8648000102C1865D.

Wachter, E.A., Hayes, J.M., 1985. Exchange of oxygen isotopes in carbon dioxide-phosphoric acid systems. Chem. Geol.: Isot. Geosci. Sect. 52, 365–374, doi: 10.1016/0168-9622(85)90046-6.

Walker, K.R., Jernigan, D.G., Weber, L.J., 1990. Petrographic criteria for the recognition of marine, syntaxial overgrowths, and their distribution in geologic time. Carbonates Evaporites 5, 141–152, doi: 10.1007/BF03174845.

Warren, J., 2000. Dolomite: occurrence, evolution and economically important associations. Earth Sci. Rev. 52, 1–81, doi: 10.1016/S0012-8252(00)00022-2.

Yaseen, M., Shahab, M., Ahmad, Z., Khan, R., Shah, S.F.A., Naseem, A.A., 2021. Insights into the structure and surface geology of balanced and retrodeformed geological cross sections from the Nizampur basin, Khyber Pakhtunkhwa, Pakistan. J. Pet. Explor. Prod. Technol. 11, 2561–2571, doi: 10.1007/s13202-021-01180-8.

Yeats, R.S., Hussain, A., 1987. Timing of structural events in the Himalayan foothills of northwestern Pakistan. GSA Bull. 99, 161–176, doi: 10.1130/0016-7606(1987)99<161:TOSEIT>2.0.CO;2.

Zenger, D., Dunham, J., Ethington, R.L., 1980. Concepts and models of dolomitization. SEPM Society for Sedimentary Geology, doi: 10.2110/pec.80.28.